平成 22 年度

三重大学大学院　生物資源学研究科

修士論文

Influence of the Antarctic sea-ice anomaly upon largescale atmospheric circulation in the Southern Hemisphere by using AGCM

大気大循環モデルを用いた南極周辺の海氷が大気循環に与える影響

Climete and Ecosystems Dynamics Division Graduate school of Bioresouces
Mie University

Ogata Koto

Supervisor:Prof. Yoshihiro Tachibana

Abstract

Interannual variation of the Antarctic dipole shaped sea-ice pattern, which is a heavy ice condition over the Pacific sector whereas a light ice condition over the Atlantic sector, is influenced by the Pacific South American Pattern (PSA pattern). This study investigates the influence of the dipole sea-ice pattern upon large-scale atmospheric circulations by using an Atmospheric General Circulation Model (AGCM), in which sea-ice boundary condition is fixed as; 1) a dipole pattern, 2) a negative dipole pattern, and 3) climatology. Comparison of atmospheric responses to the three boundary conditions can isolate the influence of the anomalous sea-ice dipole-shaped distribution upon large scale atmosphere. The result shows that the influence of sea-ice upon the atmosphere dominantly occurs in the Pacific sector than the Atlantic sector. In addition, the pattern that appears in the atmosphere is similar to the PSA pattern. Moreover, that influence makes the atmospheric amplitude lager.

1. Introduction

The sea-ice on the Antarctic ocean plays an important role in creating the ocean thermohaline circulation [Morales Maqueda et al. 2004]. The ocean thermohaline circulation is also called as the Deep circulation. Deep water is divided into the North Atlantic Deep Water and the Antarctic Bottom Water. The North Atlantic Deep Water burrow into the North Atlantic Ocean northern part. The Antarctic Bottom Water is produced in the Antarctic Ocean. Quantifying Antarctic Bottom Water is estimated to have twice the North Atlantic Deep Water volumes [Johnson 2008]. Therefore, the sea-ice on the Antarctic ocean is quite important role for world ocean circulation.

However, there are little studies about influence of the sea-ice upon the atmosphere. Because, the observation of atmosphere is very difficult in the seasonal sea-ice development. The sea-ice is made by the wind in the Antarctic winter. Interannual variation of the Antarctic dipole shaped sea-ice pattern, which is a heavy ice condition over the Pacific sector whereas a light ice condition over the Atlantic sector [Udagawa et. al. 2009], is influenced by the Pacific South American Pattern (PSA) [Karoly, 1989]. Although The Southern Hemisphere annular mode [Thompson and Wallace, 2000] or the Antarctic oscillation [Gong and Wang, 1999] (SAM/AAO) is normal mode for the Antarctic atmosphere, PSA pattern appear when El Niño year well. In this study, we will demonstrated that the influence of the sea-ice pattern upon the atmosphere by using AGCM. It is very difficult to cut off only sea-ice effect from observation data. Consequently, we change only sea-ice AGCM boundary condition. In other words, we are clearly influence of sea-ice.

2. AGCM Data and Reanalysis Data

2.1 AGCM computation environment

The Atmospheric General Circulation Model is CCSR/NIES AGCM Ver. 5.6 (Center for Climate System Research, University of Tokyo / National Institute for Environmental Studies Atmospheric General Circulation Model). The resolution is T42L20. The horizontal grid size of T42 is approximately 300 km. The atmosphere is divided into 20 layers. The calculation step is 20 minutes. The outputs are average of 12 hours. The experimentation was calculated for 55 years. The first five years were not fitted in there are atmosphere. We make three monthly mean data from that. We got the output variables that are surface pressure, zonal wind velocity, meridional wind velocity, geopotential height, temperature, sea level pressure, outgoing longwave radiation, vertical wind velocity and precipitation. Incidentally, we used zonal wind velocity, meridional wind velocity, geopotential height, temperature.

2.2 Reanalysis Data

We also used three monthly mean geopotentian data from reanalysis data. We used six hours mean atmospheric reanalysis data provided by the National Centers for Environmental Prediction/National Centers for Atmospheric Research (NCEP/NCAR) on a 2.5×2.5 degree regular latitude-longitude global grid [Kalnay et al. 1996]. This data set is available from http://dss.ucar.edu/datasets/ds090.0/. The analysis period for all of the data sets was 1958 through 2011.

The Oceanic Niño Index (ONI) shows El Niño and La Niña intensities. That is the running three month mean of ERSST.v3d SST anomalies in the Niño 3.4 region (i.e., 5° N to 5° S , 120° E to 170° W). The data was obtained from the National Oceanic and Atmospheric Administration / the extended reconstructed sea surface temperature version 3 (NOAA ERSST.v3) , which is constructed using the recently available International Comprehensive Ocean-Atmosphere Data Set (ICOADS) SST data and improved statistical methods that allow stable reconstruction using sparse data [Smith et al. 2007, Xue et al. 2003] and available online at http://www.cpc.ncep.noaa.gov/products/monitoring_and_data/ENSO_connections.shtml. The analysis period for ONI is also 1958 through 2011.

3. Method

We experimented nine AGCM sea-ice boundary conditions. The original AGCM sea-ice boundary condition, that is control run (CTL), shown in the blue area in Figure1. We changed the green area or the orange area in Figure1. The sea-ice on the green area and the orange area is set particularly when the PSA pattern develops. The Large Run A (LA)has large sea-ice boundary condition (490kg/m^2) in green area in Figure1 , whereas The Small Run A (SA) wears small sea-ice boundary condition (0kg/m^2) in orange area in Figure1 . On the other hand, the Large Run B (LB) and the Small Run B (SB) have same designation but different area. Likewise, the Large Run AB (LAB) put both areas on large sea-ice boundary condition while there is no sea-ice the

Small Run AB (SAB) in both areas. The PSA sea-ice pattern (PSA-ice) is combines Large Run A and Small Run B characteristic. The Anti-PSA sea-ice pattern (aPSA-ice) is opposite feature of PSA sea-ice pattern. For instance, sea surface temperature (SST) is adopted when there are not sea-ice (Figure2). Other, there are difference in albedo, surface roughness and momentum flux. In this study, we refer to CTL, LA, LB, SA and SB. Wintertime seasonal data, that is average of August, September and October (ASO), were mainly used. Initially, we confirm some gaps of phase. The second, we compared CTL with others. The calculation of wave-activity flux [Takaya and Nakamura, 2001] was employed to find out the origin of the atmospheric disturbances.

An empirical orthogonal function (EOF) analysis was applied to mass-weighted vertical average geopotential height anomaly data and temperature anomaly data. The EOF analysis covered an area from 20 degrees S to 90 degrees S.

Even though The El Niño event has two to seven year cycle and occurs in real atmosphere, there is not the El Niño event in the AGCM calculation environment. Hence, we needed to cut off the El Niño event from NCEP/NCAR reanalysis data. Figure3 is Niño 3.4 index in Jun to October of from 1958 to 2011. If the index exceeding threshold level continues five months, that it is called El Niño or La Niña. El Niño is when above +0.5 anomaly and La Niña is when below -0.5 anomaly. As a result, we selected 26 years (1958, 1959, 1960, 1961, 1962, 1966, 1967, 1968, 1976, 1977, 1978, 1979, 1980, 1981, 1984, 1985, 1989, 1990, 1993, 1995, 1996, 2000, 2001, 2005, 2008 and 2011).

4. Results

4.1 Comparison with CTL and wave-activity flux

Figure4 shows atmospheric variations are removed zonal mean geopotential height from each AGCM data at all level (not shown in Figure4). Each AGCM runs at all level are nearly in phase. The intensity of the phase has little difference in each other. Accordingly, the disturbances appearing comparison with CTL are not that are built by difference of phase.

Figure5 shows the anomaly of comparison with CTL at 500hPa level in ASO. They exhibit positive anomalies in the western Atlantic sector and negative anomalies in the central Pacific sector. The pattern is similar to PSA pattern (Figure7). Significant action centers of SB and LB are in the western Atlantic sector, the Bellingshausen-Amundsen Seas, and the east South Pacific. Because wave-activity flux is reckoned by the anomaly, we could become aware the origin of the disturbances. Figure6 shows that the wave-activity flux of SB and LB. The flux start from the Amundsen Sea. In other words, the flux in sea-ice boundary condition area, where was changed by AGCM runs, includes products of velocity and temperature perturbations. The change of sea-ice boundary condition produces the disturbances like a PSA pattern. SB is similar to PSA sea-ice pattern. If the PSA pattern composes small sea-ice in Amundsen Sea area, the disturbances make intense that of the PSA pattern. Oppositely, LB is resemblant to anti-PSA sea-ice pattern. If there are appearing anti-PSA pattern, that become weak by disturbances ware produced by anti-PSA sea-ice pattern.

4.2 EOF analysis

Figure7 shows the first, second and third EOFs of NCEP/NCAR atmospheric from 1958 to 2011 in ASO at 500hPa level. Hereafter, the spatial pattern of atmospheric first mode and its time series are aferred to as EOF1 and EOF1 index, respectively, and those of the second mode as the EOF2 and EOF2 index, and third mode as the EOF3 and EOF3 index. The variances contributed by EOF1, EOF2 and EOF3 are 20.4%, 17.1% and 14.1%, respectively. The spatial pattern of the first mode is similar to that of AAO/SAM, whereas the seconde mode exhibits positive anomalies in the western Atlantic sector and negative anomalies in the central Pasific sector. This is so-called the PSA pattern, which is activated by tropical anomalous heating [Hoskins and Karoly, 1981, Karoly, 1989].

Figure8 shows the EOF1 of AGCM atmospheric data. The variances contributed by CTL, LA, SA, LB and SB are 18.7%, 13.0%, 15.5%, 16.7% and 17.9%. All AGCM EOF1s appear as the AAO/SAM. Figure9 shows the EOF2 of AGCM atmospheric data. The variances contributed by CTL, LA, SA, LB and SB are 11.7%, 11.7%, 13.3%, 11.49% and 10.7%. This spatial pattern looks like the PSA pattern.

Here, we tried combination of CTL data, SB data, LA data, LB data and SA data. Then, Figure10 is EOFs that is got the calculation of the combination data (referred to as the com-EOF1, com-EOF2, com-EOF2 index). The com-EOF1 is resemble the AAO/SAM than the EOF1s. That’s mean AGCM model, which have a variety of sea-ice boundary conditions, design natural atmosphere than CTL. Focusing attention on the com-EOF2 indexes exhibit the atmosphere is barotropic. Because the

com-EOF2 index is difference AGCM runs each 50 years, we focused respectively. Every AGCM runs created atmospheric fluctuation. The averages of CTL and SB are positive, on the one hand, LA, LB and SA are negative. The variance of SB, LB and SA are axiomatically greater than CTL variations. That mean, The AGCM runs changed in sea-ice area pull out the atmospheric oscillation.

4.3 Comparison with AGCM data and Reanalysis data without El Niño events

Niño3.4index in Jun to October of from 1958 to 2011 (Figure3) discriminate between El Niño/La Niña years and normal years. We chose years that above +0.5 anomaly and below -0.5 anomaly. Likewise, we calculated EOF of NCEP/NCAR in those years which are Figure12 (referred to as No-ENSO EOF1 and No-ENSO EOF2, respectively). The variances contributed by No-ENSO EOF1 and No-EOF2 are 25.2% and 18.17%. The variances contributed by No-ENSO EOF1 are higher than EOF1. No-ENSO EOF2 is more similar to com-EOF2 than EOF2. The points that AGCM runs present the natural atmosphere without ENSO. Approach the subject from a different perspective, the No-ENSO EOF2 is alike the EOF3. In fact, the EOF3 suggests the pattern contain a high proportion of influence of sea-ice anomaly.

5. Discussion and Conclusion

The previous study confirmed the PSA pattern make the spatial pattern of sea-ice concentration [Udagawa et al. 2009]. This study verified the opposite process. In this study, we ran AGCM runs

which changed sea-ice boundary conditions. One is there are no sea-ice on the Atlantic sector. Another one is there are full sea-ice boundary condition on that area. And other two runs which has similar sea-ice boundary condition on the Pacific sector. The remaining runs are those combinations of sea-ice boundary condition. We investigated the influence of the sea-ice anomaly upon atmosphere by comparing control run and the changed boundary condition AGCM runs. The composing of small sea-ice in Amundsen Sea area make the disturbances intense that of the PSA pattern. While LB is resemblant to negative the PSA sea-ice pattern. The anti-PSA pattern has sea-ice formed as the anti-PSA sea-ice pattern. But the sea-ice pattern become weak the anti-PSA pattern by formation of the PSA pattern. The EOF analysis index of the combination of AGCM runs which are changed in sea-ice area suggest that the largescale atmospheric oscillation is pulled out by sea-ice anomaly. In conclusion, the influence of the sea-ice anomaly has asymmetry response between the large sea-ice area and the small sea-ice area.

The disturbance like the PSA pattern which occurring AGCM runs that changed sea-ice boundary condition propagate from predominately the Amundsen Sea. That is related by wave-activity flux from the Amundsen Sea above the Antarctic Peninsula to the Atlantic sector.

Further studies on the mechanism of the influence must be examined in future.

6. Acknowledgements

I am deeply grateful to Prof. Tachibana whose enormous support and insightful comments were invaluable during the course of my study.

Special thanks also go to Mr. Udagawa and Ph.D Oshima and Mr. Yoshida whose meticulous comments about AGCM were an enormous help to me.

I would also like to express my gratitude to members of ecosystems dynamics laboratory, geosystem science in factory of bioresources at Mie University and my family for their moral support and warm encouragements.

7. Reference

Gong, D.-Y., and S.-W. Wang (1999), Definition of Antarctic oscillation index. Geophy. Res. Lett., 26, 459–462.

Hoskins, B. J., and D. J. Karoly (1981), The steady linear response of a spherical atmosphere to thermal and orographic forcing, J. Atmos. Sci., 38, 1179-1196.

John sin, G C. : Quantyfying Antarctic Bottom Water and North Atlantic Deep Water volumes, J. Geophys. Res., 113, C05027

Kalnay, E., et al. (1996), The NCEP/NCAR 40-year reanalysis project, Bull. Am. Meteorol. Soc., 77, 437–471.

Karoly, D.J. 1989, Southern Hemisphere circulation features associated with ElNiño–Southern Oscillation Events, J. Climate, 2, 1239-1252.

Morales Maqueda, M. A., A. J. Willmott, and N. R. T. Biggs (2004), Polynya dynamics: A review of observations and modeling, Rev. Geophys., 42, RG1004, doi:10.1029/2002RG000116**.**

Smith, T. M.; R. W. Reynolds; T. C. Peterson; J. Lawrimore. Improvements to NOAA's Historical Merged Land-Ocean Surface Temperature Analysis (1880-2006). Journal of Climate. In press.

Takaya, K., and H. Nakamura (2001), A formation of a phase-independent waveactivity flux for stationary and migratory quasigeostrophic eddies on a onally varying basic flow. J. Atmos. Sci., 58, 608–627

Thompson D. W. J., and J. M. Wallace (2000), Annular Modes in the Extratropical Circulation. Part I: Month-to-month variability. J. Climate, 13, 1000–1016.

Y. Udagawa, Y. Tachibana, and K. Yamazaki (2009), Modulation in interannual sea ice patterns in the Southern Ocean in association with large‐scale atmospheric mode shift, J. Geophys. Res., 114, D21103, doi:10.1029/2009JD011807.

8. Figure captions

Figure 1.

The Sea-ice boundary condition of AGCM for JAN-DEC (blue area). The sea-ice boundary condition on green and orange area were changed in some AGCM runs.

Figure 2.

The sea surface temperature boundary condition of AGCM for JUN-NOV. There are not the sea-ice boundary condition where in the green line and the orange line in some AGCM runs. If there is not sea-ice, that the AGCM calculation use sea surface temperature for bottom boundary condition.

Figure 3.

Index of El Niño and La Niña intensities on each 54 years in Jun to October between 1958 and 2011. The data use Oceanic Niño Index data by three month mean of ERSST.v3d SST anomalies in the Niño 3.4 region (i.e., 5°N to 5°S , 120°E to 170°W).

Figure 4.

The spatial pattern of (a) CTL, (b) LA, (c) LB, (d) SA and (e) SB for ASO mean geopotential height anomalies from each zonal average at 500hPa level. The unit for the shading is m.

Figure 5.

The spatial patterns of (a) SB, (b) LB, (c) LA and (SA) for ASO mean geopotential height anomalies from CTL at 500hPa. The contours are anomalies and shades indicate 80% over statistical confidence based on t-tests.

Figure 6.

The same as Figure 5(a) and (b), expect for the vector are wave-activity flux respectively.

Figure 7.

(top) The spatial patterns of (a) EOF1, (b) EOF2 and (c) EOF3 for ASO mean geopotential height anomalies from 20° S to 90° S for 5-55. See the text for details on the calculation method. (bottom) Corresponding time series of the first (black line), second (blue line) and third (green line) modes. The values are standardized. Shading in (a) and (b) indicates the linear regression coefficients for the mass-weighted geopotential height field with the time series of the first and second modes, respectively.

Figure 8.

The same as Figure 7(top (a)),expect for the EOF calculation by AGCM runs data. The variances contributed by the AGCM EOF1(a), AGCM EOF1(b), AGCM EOF1(c), AGCM EOF1(d) and

AGCM EOF1(e) are 18.7%, 13.0%, 15.5%, 16.7% and 17.9%, respectively.

Figure 9.

The same as Figure 8, expect for the EOF2 of the EOF calculation by AGCM runs data. The variances contributed by the AGCM EOF2(a), AGCM EOF2(b), AGCM EOF2(c), AGCM EOF2(d) and AGCM EOF2(e) are 11.7%, 11.7%, 13.3%, 11.49% and 10.7%, respectively.

Figure 10.

The same as Figure 7, expect for the EOF2 of the EOF calculation by AGCM runs combination data which CTL, SB, LA, LB and SA. The spatial pattern of (a) com-EOF1 at 500hPa level, (b) com-EOF2 at 700hPa level and (c) com-EOF2 at 200hPa level. (b) The red line at the bottom of the figure represents the second mode at 700hPa level while CTL, (c) the blue line represents the second mode at 500hPa level and (d) the green line represents the second mode at 200hPa level.

Figure 11.

Variance of time series of com-EOF2 respectively.

Figure 12

The same as Figure 7(top (b)), except for the EOF calculation only for 1958 - 1962, 1966 - 1968,

1976, - 1981, 1984, 1985, 1989, 1990, 1993, 1995, 1996, 2000, 2001, 2005, 2008 and 2011. The variances contributed by No-ENSO EOF1 and No-EOF2 are 25.2% and 18.17%.

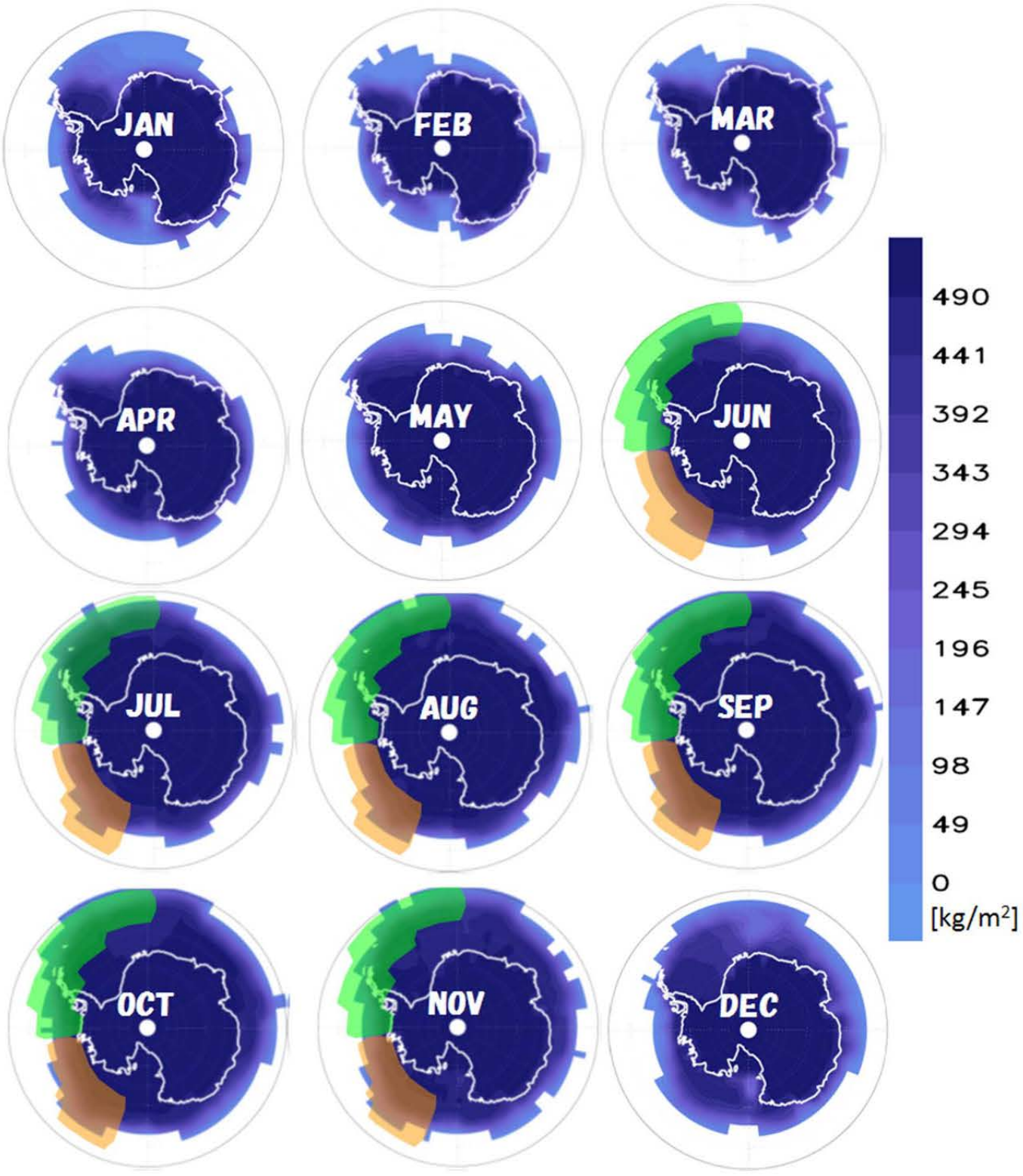
JAN
FEB
MAR
APR
MAY
JUN
JUL
AUG
SEP
OCT
NOV
DEC
490
441
392
343
294
245
196
147
98
49
0
[kg/m²]

Figure1.

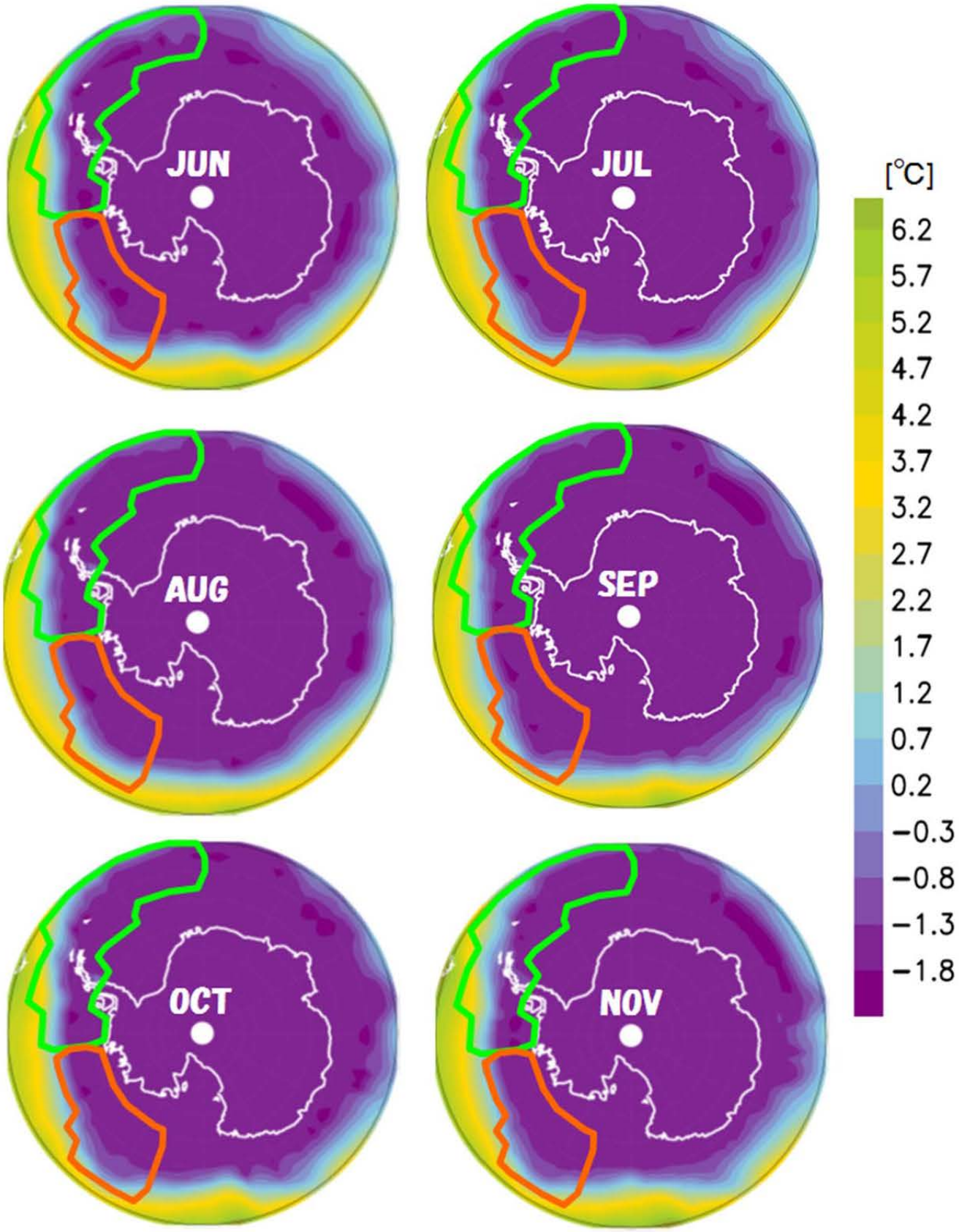
JUN
JUL
AUG
SEP
OCT
NOV
[°C]
6.2
5.7
5.2
4.7
4.2
3.7
3.2
2.7
2.2
1.7
1.2
0.7
0.2
−0.3
−0.8
−1.3
−1.8

Figure2.

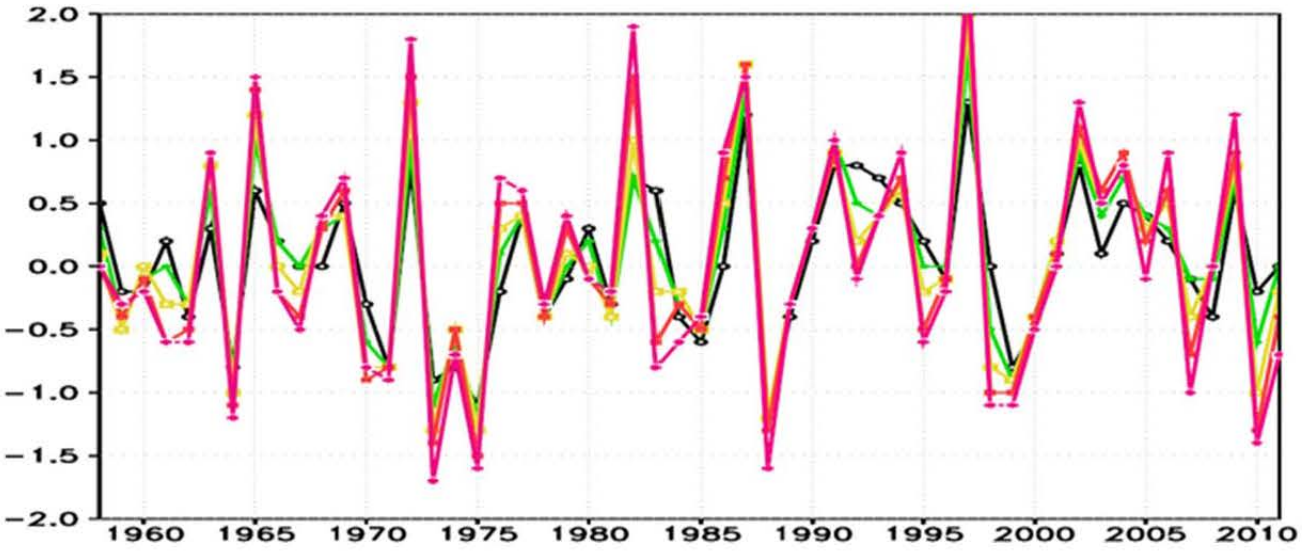
2.0
1.5
1.0
0.5
0.0
−0.5
−1.0
−1.5
−2.0
1960
1965
1970
1975
1980
1985
1990
1995
2000
2005
2010

Figure3.

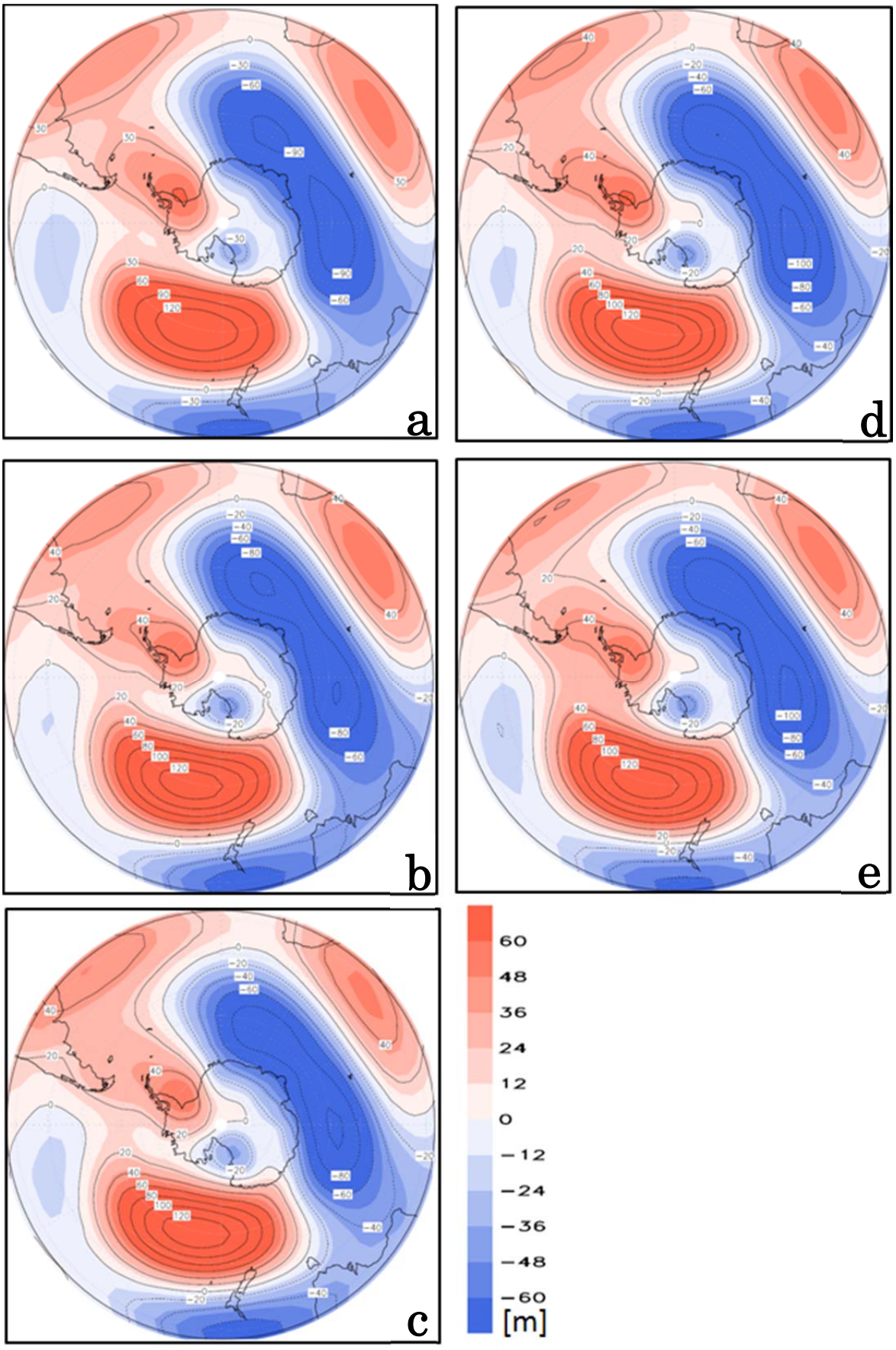

Figure4.

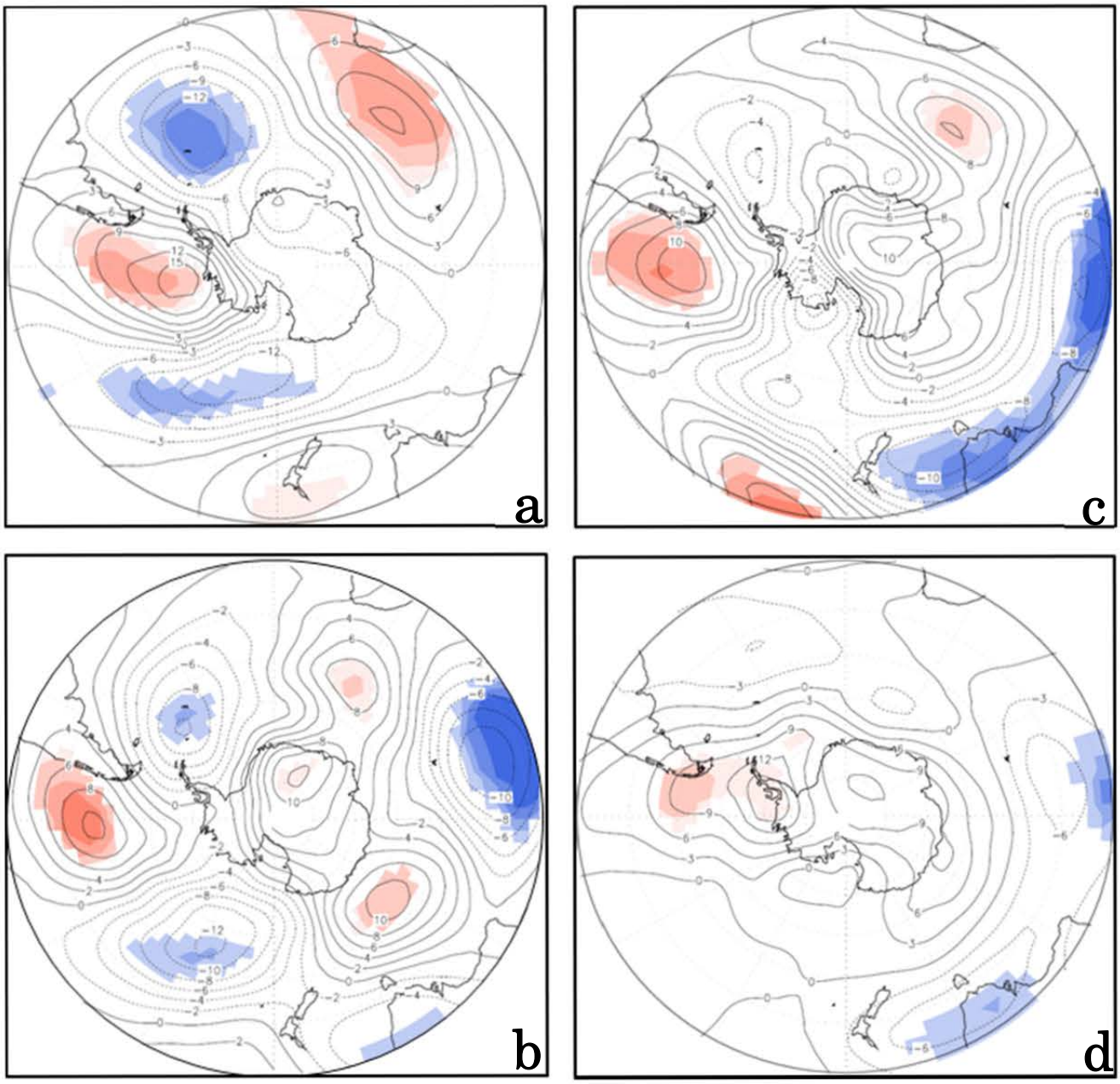

Figure5.

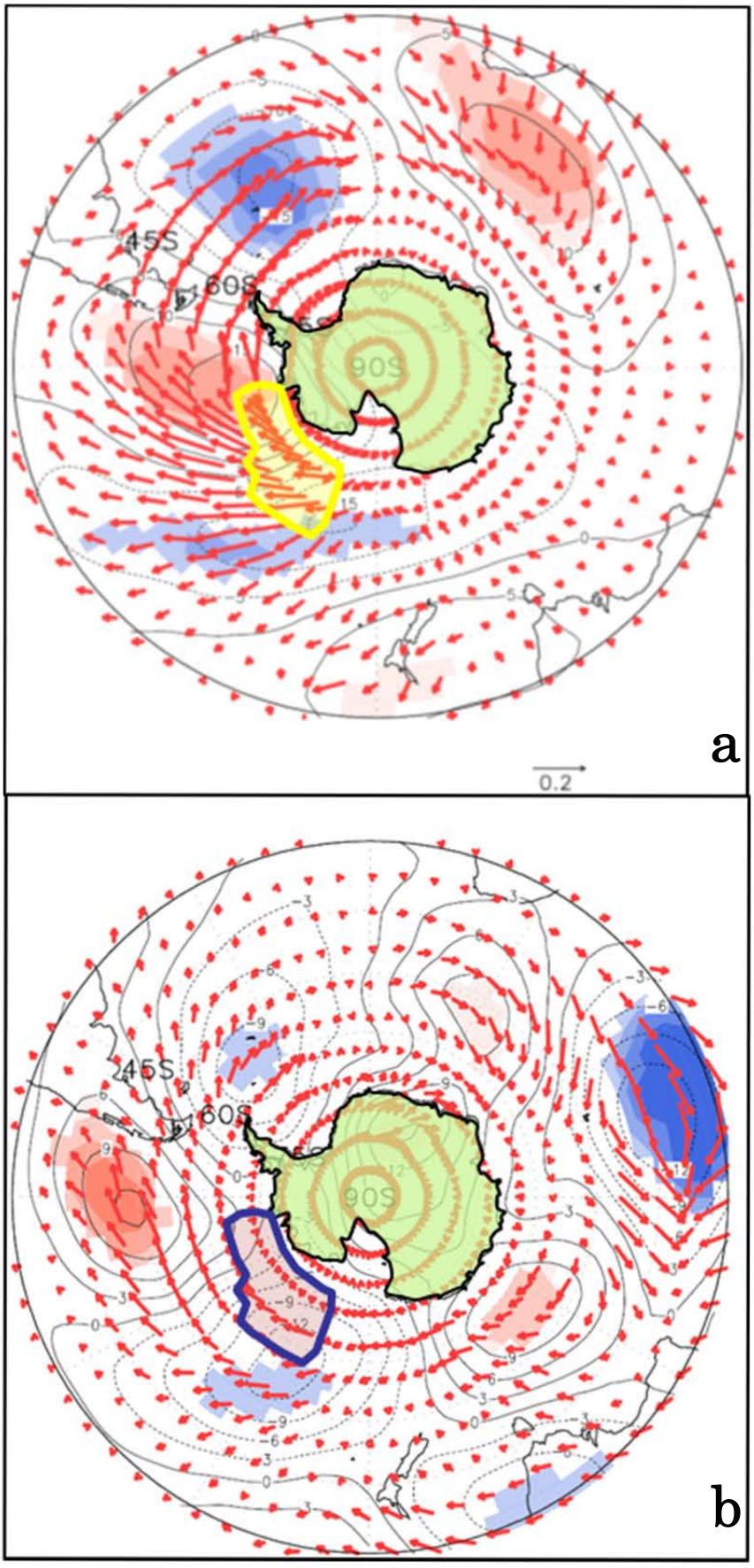

Figure6.

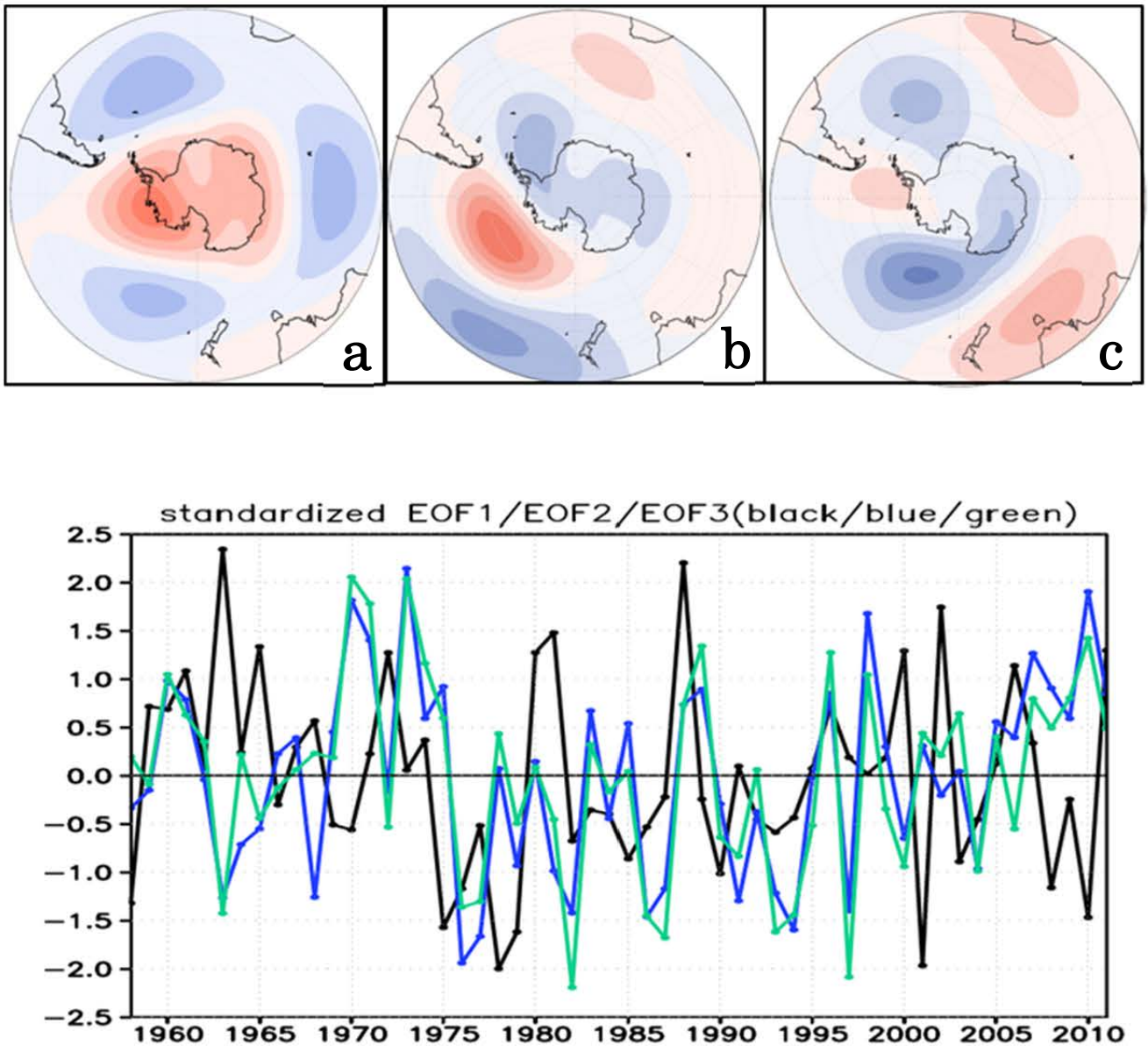
a
b
c
standardized EOF1/EOF2/EOF3(black/blue/green)
2.5
2.0
1.5
1.0
0.5
0.0
−0.5
−1.0
−1.5
−2.0
−2.5
1960
1965
1970
1975
1980
1985
1990
1995
2000
2005
2010

Figure7.

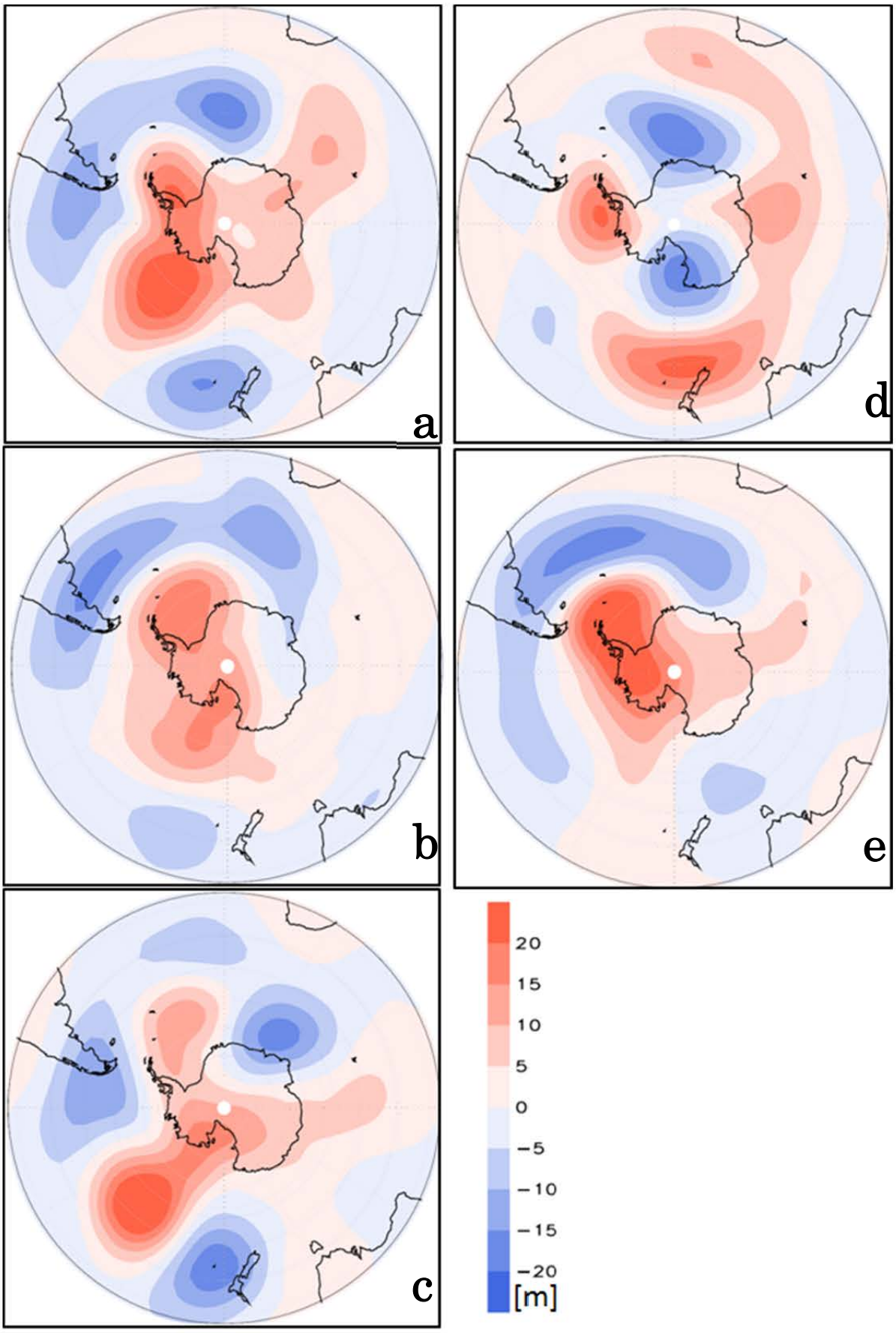

Figure8.

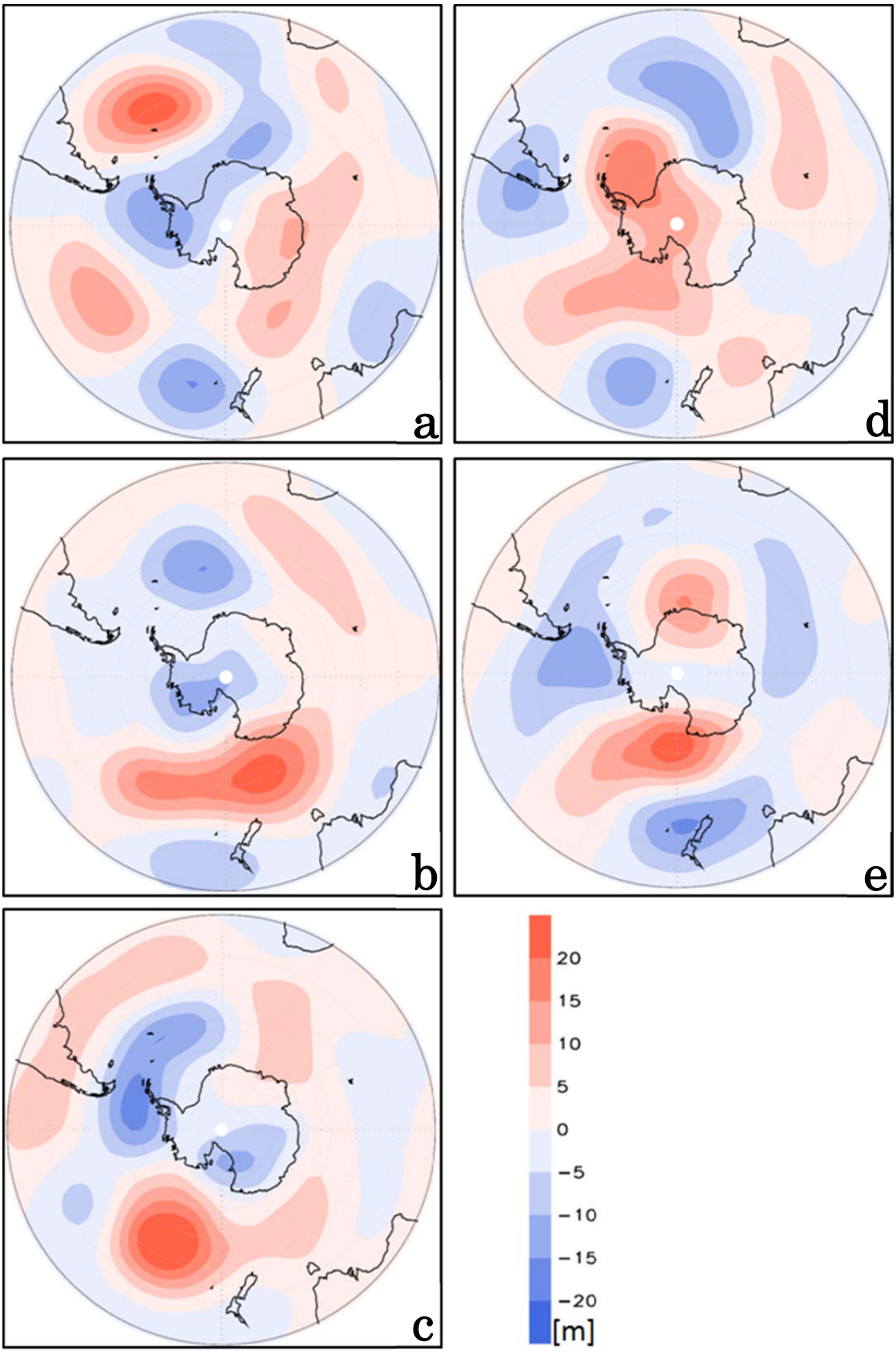

Figure9.

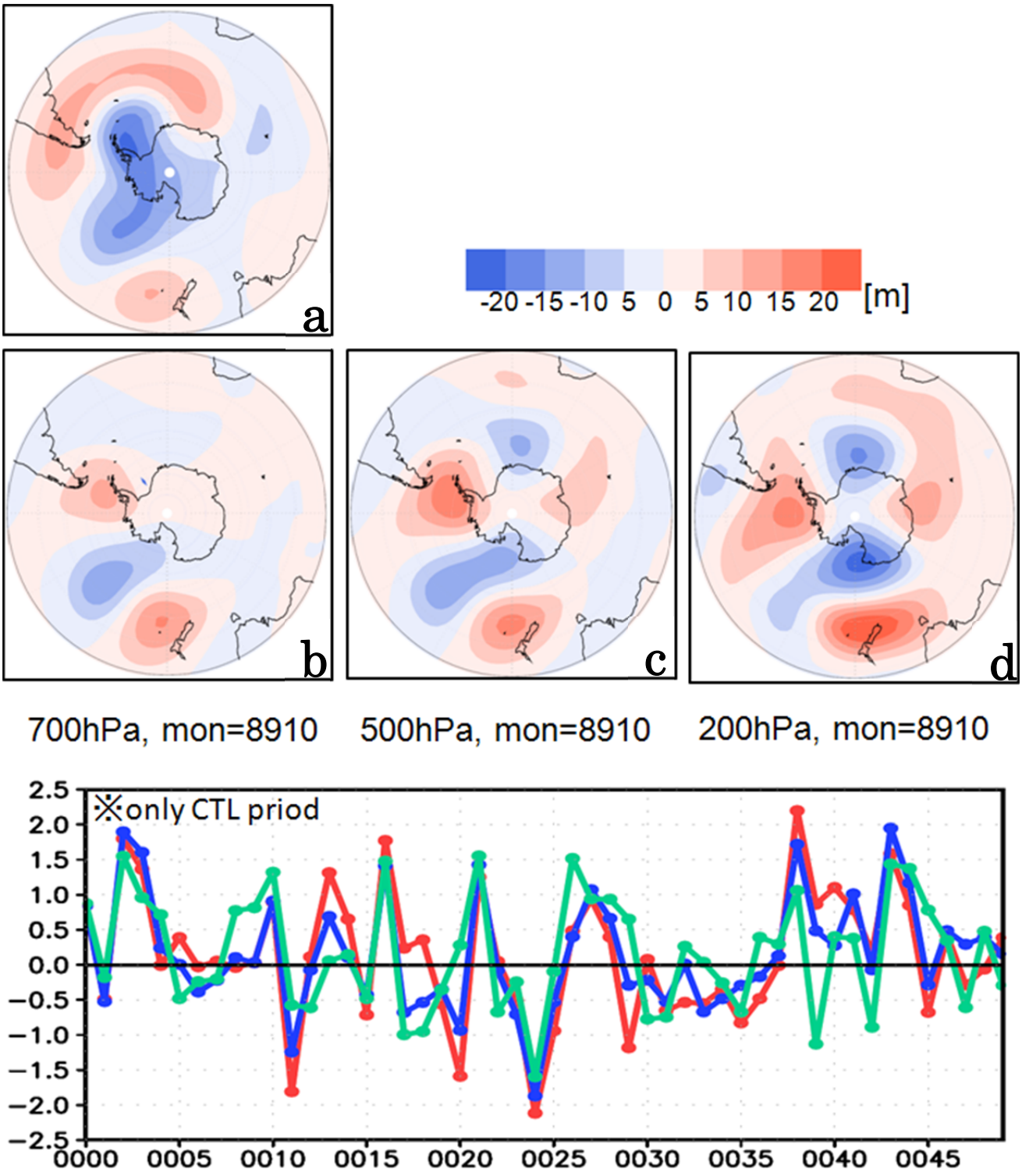
a
b
c
d
-20 -15 -10 5 0 5 10 15 20 [m]
700hPa, mon=8910
500hPa, mon=8910
200hPa, mon=8910
※only CTL priod
2.5
2.0
1.5
1.0
0.5
0.0
−0.5
−1.0
−1.5
−2.0
−2.5
0000 0005 0010 0015 0020 0025 0030 0035 0040 0045

Figure10.

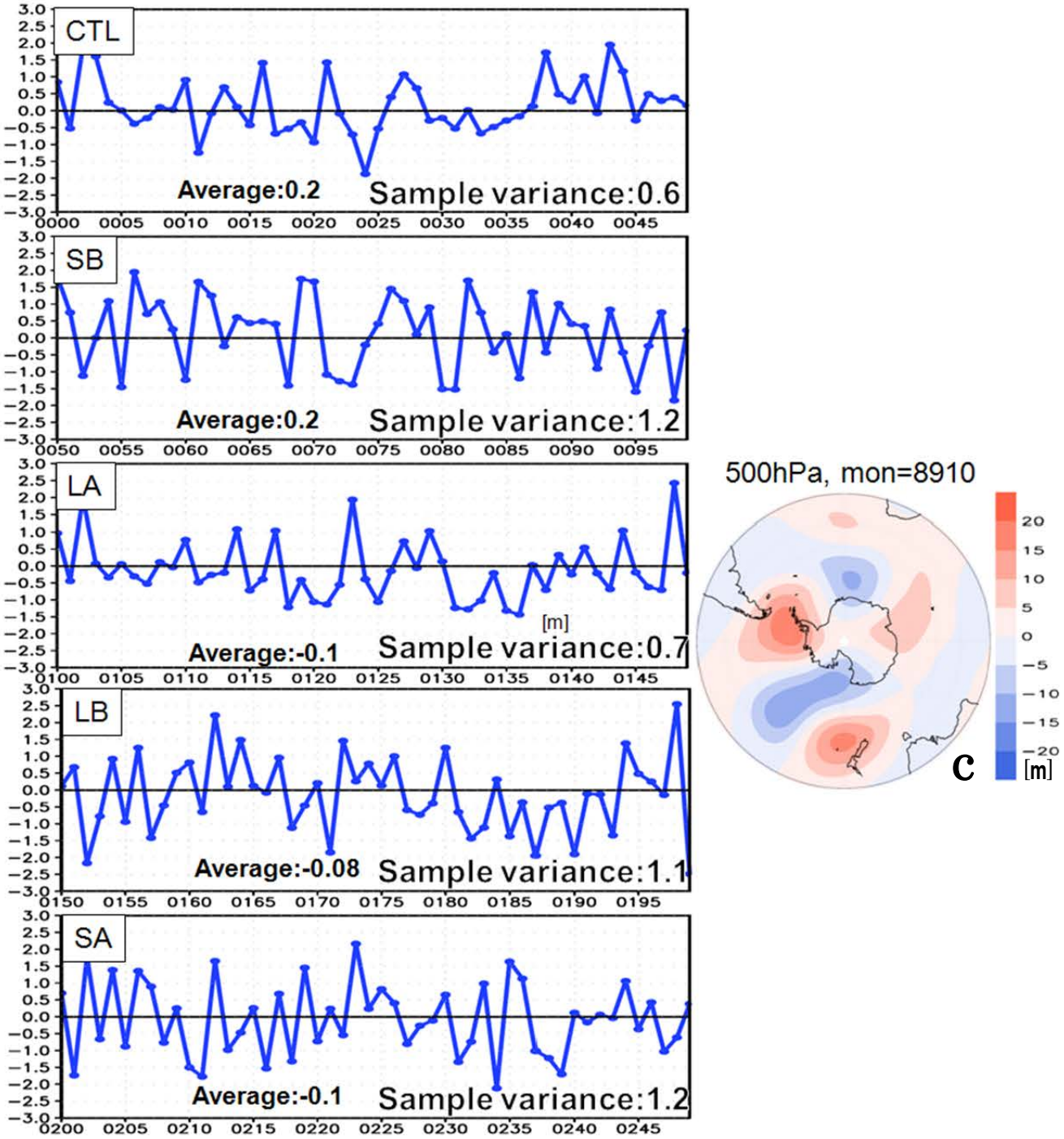
CTL
Average:0.2
Sample variance:0.6
SB
Average:0.2
Sample variance:1.2
LA
[m]
Average:-0.1
Sample variance:0.7
LB
Average:-0.08
Sample variance:1.1
SA
Average:-0.1
Sample variance:1.2
500hPa, mon=8910
C
[m]

Figure11.

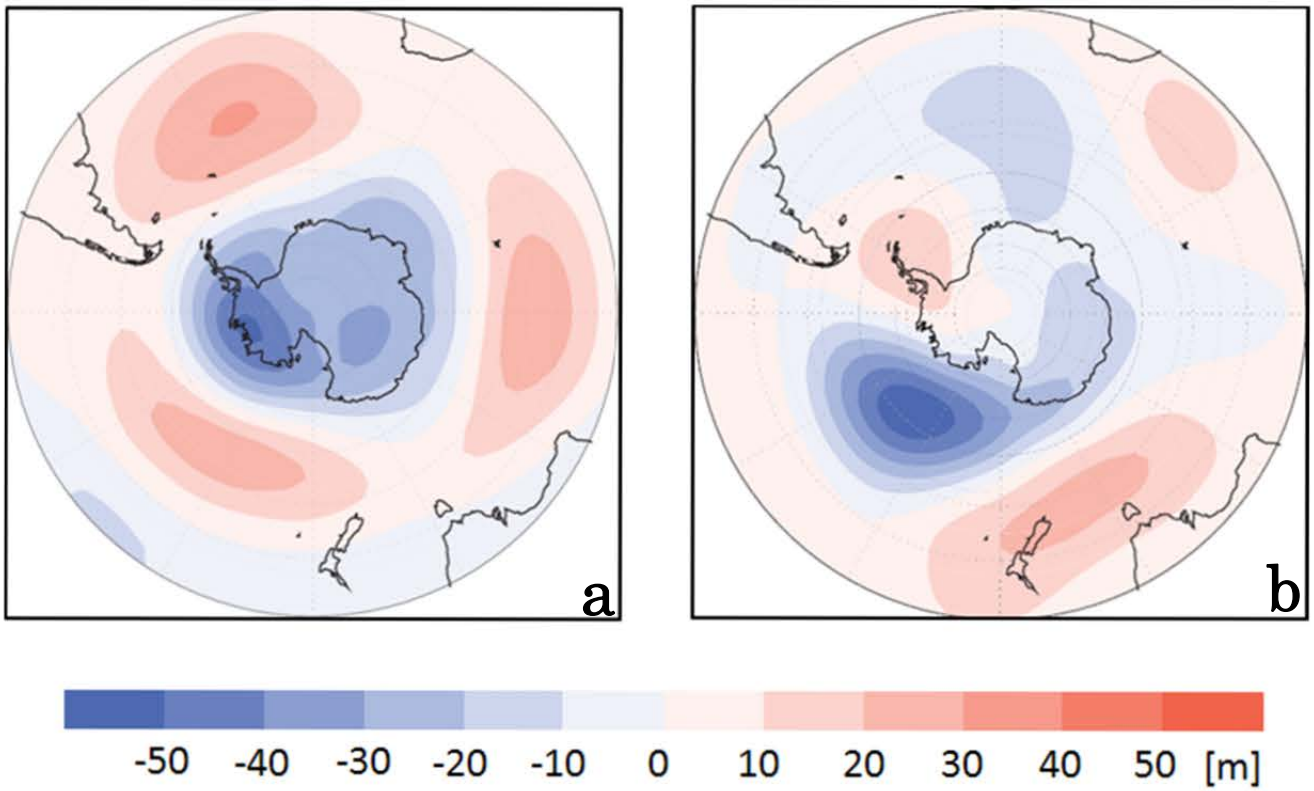

Figure12